

HYDRODYNAMIC MODELLING STUDY OF A ROTATING LIQUID SHEET CONTACTOR

Christopher B. SOLNORDAL^{1*} Andrew ALLPORT² and Leigh T. WARDHAUGH³

¹ CSIRO Mineral Resources, Clayton, Victoria 3169, AUSTRALIA

² CSIRO Services, Newcastle, 2300, AUSTRALIA

³ CSIRO Energy, Newcastle, 2300, AUSTRALIA

*Corresponding author, E-mail address: chris.solnordal@csiro.au

ABSTRACT

The Rotating Liquid Sheet contactor is a recently developed gas-liquid contactor capable of providing high interphase contact in combination with a low associated pressure drop of flowing gas. The device consists of a cylindrical flow passage and a central rotating tube with helical slots in its walls. Liquid passes into the central tube and out through the slots, forming continuous sheets of liquid in the shape of helices or compressor blades, depending on the slot design. Gas passes through the annular gap between the cylinder and central tube. By rotating the central tube, the liquid sheets provide high surface area for interphase contact while simultaneously pumping gas through the device. In order to optimise design of the unit, computational fluid dynamics has been used at many stages of the development process. This paper describes attempts to model the gas flow through the unit, the liquid flow through the central tube, and the dynamics of the liquid sheet. It was found that the unit is capable of pumping gas through it using the helical liquid sheet. Also profiled struts along the slots were required to produce a uniform horizontal flow of liquid through them. An extremely fine mesh was required to allow modelling of the liquid sheet. The stability of the predicted liquid sheet was found to be highly sensitive to the specified surface tension. However, by using a surface tension value lower than the standard value for water, a uniform sheet with parabolic profile was predicted, as was observed experimentally.

INTRODUCTION

Traditional packed column gas-liquid contactors are a mature technology that offer little in the way of potential process improvements. Increasing gas flow causes liquid entrainment, while gravity-fed liquid flow rate is limited by the liquid viscosity. A novel type of gas-liquid contactor is the Rotating Liquid Sheet (RLS) contactor, recently developed and patented by the authors (Wardhaugh *et al.* 2012, Wardhaugh *et al.* 2015). The RLS contactor creates a sheet of liquid within a cylindrical flow passage. The sheet surface is that of a number of continuous helices or else short blade-like surfaces, so that when rotated the liquid surface pumps gas through the device, in a manner similar to a screw conveyor. The system is shown schematically in Figure 1a for a single continuous helical liquid sheet. Figure 1b shows a photograph of an air-water laboratory scale model of the

contactor where the stability of the liquid sheet is visible for the conditions studied. Features of the photograph are identified in Figure 1c. Compared to a packed column, the RLS contactor allows increased gas throughput with negligible liquid entrainment in the gas stream, and the use of higher viscosity liquids. Furthermore, the pumping action of the liquid sheet decreases the pressure loss for gas passing through the system.

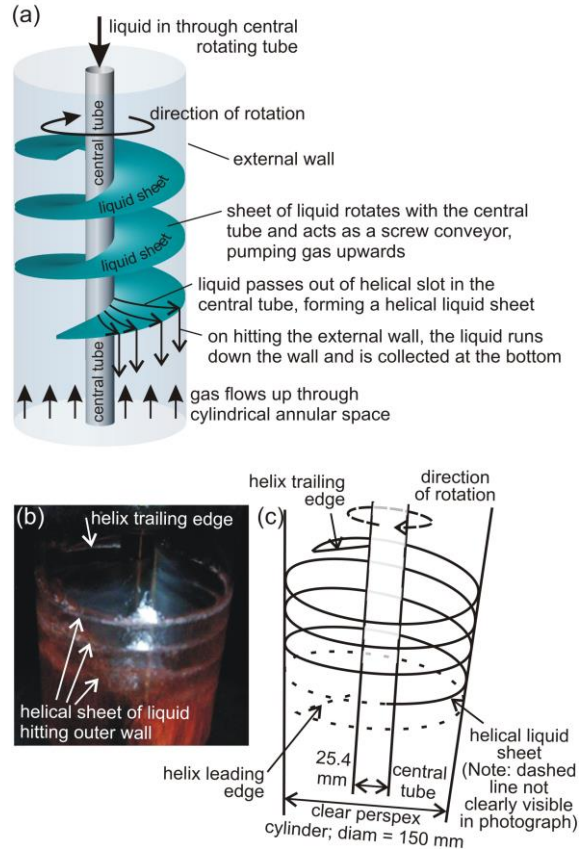


Figure 1: (a) Schematic diagram of RLS contactor; (b) photograph of liquid film; (c) diagram explaining features in photograph.

In order to understand and optimise the fluid mechanics of the RLS contactor, CFD modelling has been used extensively. However, the complexity of the system meant that it was difficult to model the entire unit at once, so instead three separate models were used to investigate different aspects of the contactor design. The feasibility of pumping gas through the unit was initially investigated

using a single phase model where the liquid sheet was modelled as a solid helical surface. The flow through the central tube and helical slot was modelled as a single liquid phase to investigate slot design. Finally, the dynamics of the liquid sheet itself was explored using a two phase air-water model extending from the helical slot to the outer wall of the device. Each of the three models was developed using Eulerian analyses within ANSYS CFX (ANSYS 2013), and are presented in turn.

CFD MODEL 1 – SOLID HELICAL SURFACE

The purpose of the solid helical surface model was to investigate the gas flow dynamics through a rotating helix, and to determine if such a helix could induce flow through it purely by rotation.

Geometry, Mesh and Boundary Conditions

The solid helical surface model geometry is represented by the schematic diagram of the RLS contactor in Figure 1a. The flow domain had a central tube outer diameter of 25.4 mm and an external wall inner diameter of 150 mm (Figure 1c) and extended 2 m upstream and 2 m downstream of the single solid helical surface. Such distances were required to ensure boundaries did not interfere with the action of the rotating solid surface on the gas flow. The solid helical surface represented the liquid sheet, and turned six times around the central tube at a pitch of 23.2 mm, with uniform thickness of 0.7 mm.

The fluid for this model was air at room temperature and pressure, with standard properties. Pressure boundaries ($P = 0 \text{ Pa g}$) were specified at the inlet and outlet of the domain, while the inner and outer walls as well were modelled as no-slip walls. It was not clear whether a no-slip or free-slip boundary would best represent the fluid interaction at the solid helical surface, since in reality the helix is a flowing liquid. A no-slip condition was used in the first instance, while comparison to free-slip or other conditions at this surface was left for future work. A 1 mm gap was left between the external wall and the solid helical surface, and a hexahedral mesh was imposed on the flow domain in such a way that the central tube and solid helical surface could rotate within the thin outer shell that represented the external wall. The mesh had a total of approximately 1.2 million elements, which were concentrated around and immediately upstream and downstream of the helical blade.

Although many runs were performed, varying both vane pitch and rotation rate, here the results are presented for pitch of 23.2 mm and rotation speed of 600 RPM. Transient simulations were performed using a time step equal to 0.008333 s, which corresponded to a centrebody rotation of 30° . A total of 120 time steps were calculated, to simulate 10 full revolutions of the centrebody. During the simulation the longitudinal flow field remained steady, suggesting that the 10 revolutions was adequate to capture the detail of the flow.

Results

The predicted instantaneous velocity profile in a vertical plane centred on the geometry axis is shown in Figure 2. Figure 2a shows the elevation view between two successive surfaces approximately half way up the helix. The distribution did not vary greatly from the lower to the upper sections of the 6-turn surface, and a reasonably steady upward velocity is predicted. Higher velocities are

shown at larger radii, but this is primarily due to the drag between the air and the solid vane causing increased tangential velocity. This behaviour is shown in Figure 2b (air velocity vector profile in plan view – distribution profile shown by white line), where velocity increases slightly with radial position. The black line in Figure 2b indicates the velocity profile of the solid vane surface, and the air velocity is only approximately 20-30% of this value. Thus the amount of swirling motion imparted to the air is small compared to the actual rotational velocity of the vane. In the real system the drag between the liquid sheet and the gas is likely even smaller since the “no slip” condition imposed here may not apply. Figure 2a also shows the existence of a recirculation trailing the outer edge of the solid vane, near the outer wall of the device. Such a flow is likely to occur on the actual device since there would be upward flow of gas in the main bulk of the flow passage but downward flow of liquid at the outer surface, thus forcing a recirculatory flow.

At the rotation rate of 600 RPM the bulk vertical velocity is predicted to be 0.177 m s^{-1} , which is 76% of the value expected if the vane were to transport the fluid as a solid body.

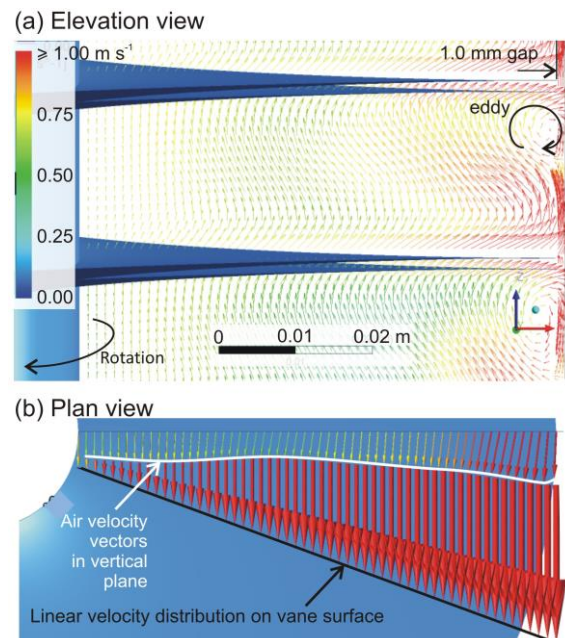


Figure 2: Velocity vector plot for flow through rotating solid helical surface model. Rotation speed = 600 RPM.

CFD MODEL 2 – CENTRAL TUBE

The purpose of the central tube model was to determine a design that could produce a uniform horizontal flow of fluid through the helical slot(s). This is important because if the flow is uneven, then successive layers of the helical film may fall onto those beneath, decreasing the available interfacial surface area for mass transfer and potentially reducing the pumping efficiency of the device. Many different geometries were investigated, and some typical ones are presented in this section (see Figure 3).

Geometry, Mesh and Boundary Conditions

The flow through the central tube was modelled primarily as a single phase, with the fluid being water at

room temperature (although some two-phase air-water modelling did take place). A typical geometry is shown in Figure 3a, where a single slot at angle of 45° to the tube axis completes a single rotation around the tube wall. The outer and inner diameters of the tube are labelled, and equal to 25.4 mm and 22.2 mm respectively, producing a wall thickness of 1.6 mm. The full geometry extends vertically a total length of 250 mm, although the entrance length is not shown in the Figure; fluid enters from above and the bottom surface is solid so that all fluid is forced through the helical slot. In this case the slot width is 1.2 mm. Images in Figure 3b-d show examples of changing slot width and profile, changing wall thickness, inclusion of a central rod and modifying its longitudinal profile, the use of multiple helical slots, short rows of multiple “blade”-like slots, helical structures on the central rod, and horizontal ribs through the slot to act as flow straighteners.

Inlet velocities were specified to provide a given average outlet velocity through the slot that varied from 1 m s^{-1} to 5 m s^{-1} . The effect of rotation was also investigated (although results are not reported here). All walls were treated as no-slip boundaries, while the inlet was a simple Dirichlet boundary and the slot outlet had a constant pressure boundary of 0 Pa g applied. Simulations were performed under steady state conditions on a tetrahedral mesh with wall inflation. Eight cells were used across the slot, and all geometric features shown in the figures were explicitly meshed. Each mesh had approximately 3 million elements.

Results

Predicted flow patterns for four selected centrebody geometries are presented in Figure 4. Figure 4a shows streamlines coloured by speed of water. The standard single slot geometry A demonstrates significant recirculation of fluid, while use of a central rod in geometry C leads to a more uniform vertical flow of fluid and less recirculation, albeit at a higher velocity due to the decreased cross-sectional area. The flow uniformity is improved further using geometry F which has four helical slots through a thicker wall, and a central rod. However, geometry F also shows streamlines travelling at a significant downward angle through the slots rather than horizontally outwards. Geometry I attempts to alleviate this flow feature by using three rows of four short slots, each of which has guide vanes positioned to attempt to create a more uniformly horizontal flow pattern at the slot outlet. The geometry appears to achieve this to some extent. In Figure 4b the velocity vector field at the slot outlets are shown for each geometry, and the vectors are coloured by the local vertical component of velocity. In all cases there is a tendency for flow to exit the slots in a downward direction (green-blue to blue vectors), and this is most pronounced for Geometry F. Geometry I is predicted to produce a more horizontal throw of fluid. Despite the promising flow field predicted for geometry I, experimental tests using such a geometry (created using additive manufacturing) showed that this bladed geometry produced many liquid sheet edges that tended to curl in towards the centre of the sheet. Therefore, ongoing work is now considering the use of continuous sheets.

Also of interest is for the centrebody to produce a uniform flow along the length of the slot. To investigate this behaviour the slots for geometries A-E (as well as some others not shown) were divided into eight equal

segments, numbered 01 (at the top of the slot) to 08 (at the bottom, see Figure 1c).

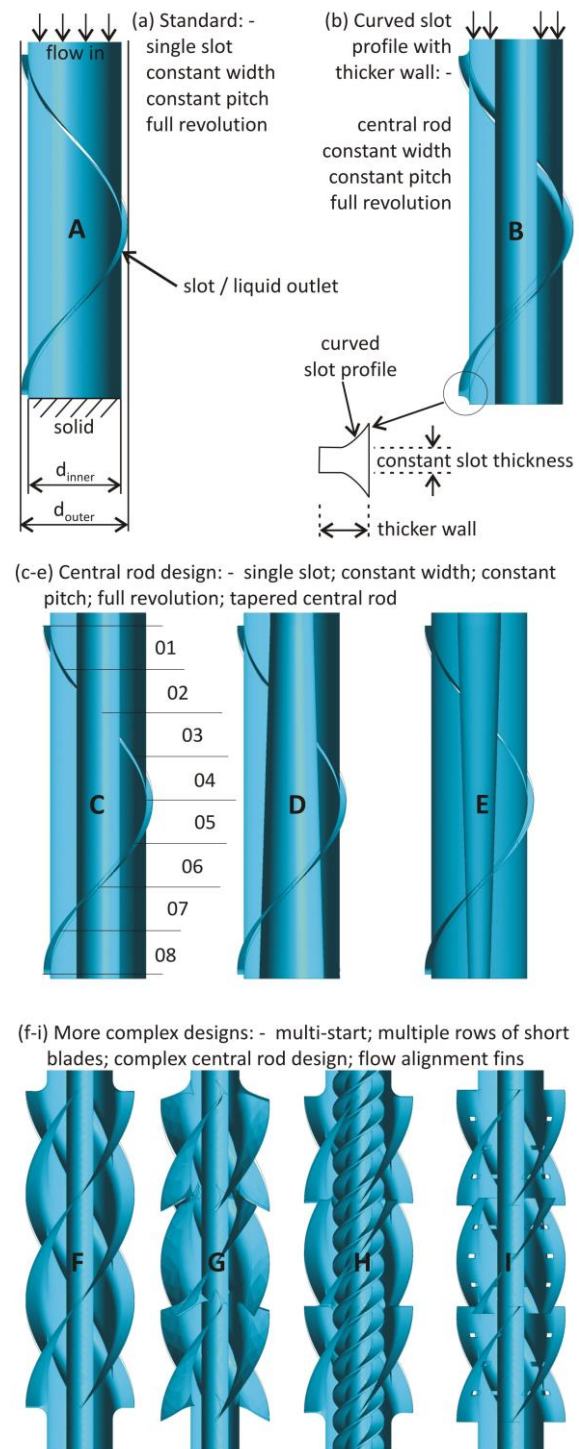


Figure 3: Different centrebody designs, labelled A-I.

The flow rate (expressed as a Reynolds number using slot width as the length scale) is plotted as a function of outlet location in Figure 5, and for all geometries studied the Reynolds number generally increased with downstream distance, although there was a slight tendency for the maximum flow to occur at outlet 06 rather than outlet 08. Geometries that used a greater wall thickness tended to give a greater variation in Reynolds number along the

length of the slot, due to the increased resistance to flow that such a geometry provided.

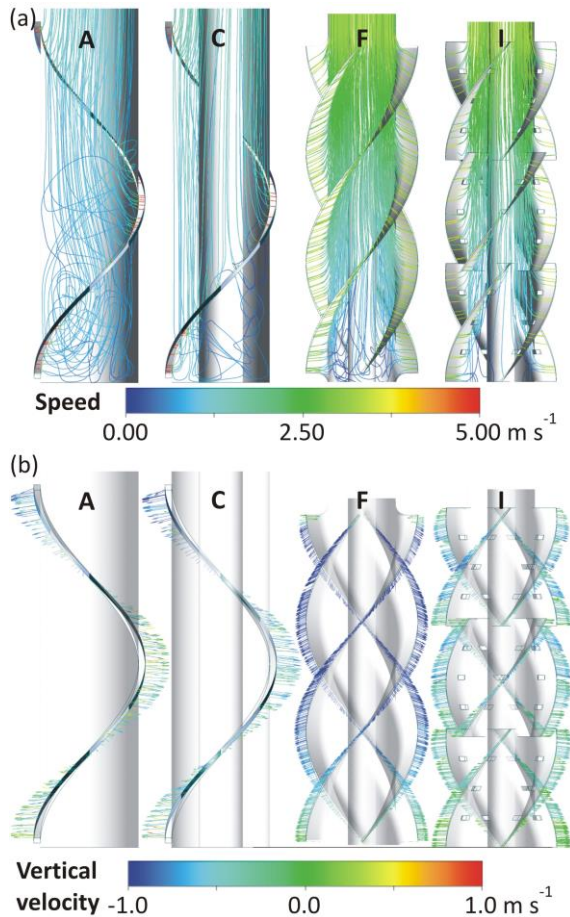


Figure 4: (a) Streamlines coloured by speed of water, and (b) velocity vectors at outlet slots coloured by vertical component of velocity, for four different centrebody geometries (A, C, F and I).

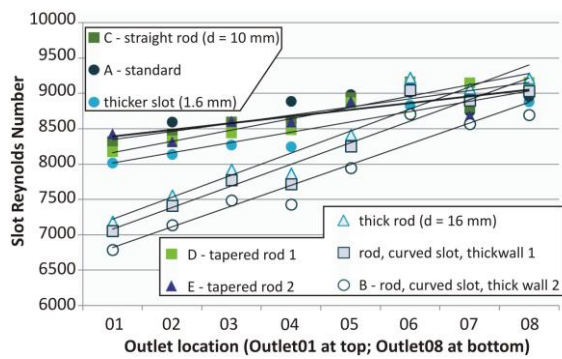


Figure 5: Variation in slot Reynolds number from top to bottom of slot, for different centrebody designs, including designs A-E as well as others not shown in Figure 3.

CFD MODEL 3 – LIQUID SHEET

The liquid sheet model was used to investigate the flow dynamics of the liquid sheet itself, as well as model the momentum transfer to the gas. In the first instance however, the aim was to determine if modelling of such a thin sheet of liquid passing through a gas was even feasible using the Eulerian-Eulerian two-phase free

surface implementation within ANSYS CFX. ANSYS CFX uses a compressive differencing scheme for determining the advection of volume fraction, combined with a compressive transient scheme for the volume fraction equations (ANSYS 2013), in an attempt to keep the gas-liquid interface sharp. Initial investigations of unbounded thin films using ANSYS CFX showed promising results, so an attempt was made to use it for modelling the current problem.

Geometry, Mesh and Boundary Conditions

The nature of a thin liquid sheet in an annular space is such that the sheet will become thinner at larger radii. This occurs because the radial velocity remains essentially constant, and mass continuity must be maintained. At a certain point the surface tension forces will overcome the momentum forces and the sheet will break up first into ligaments, and then into droplets (Dombrowski and Johns 1963). In order to capture the surfaces on either side of the sheet, a very fine mesh was necessary, so a 60° segment of the flow domain was modelled to limit the number of mesh elements required. Furthermore, the flow domain only extended 10 mm above and below the liquid sheet, and even using such a small domain the hexahedral mesh consisted of approximately 3 million elements. Figure 6 provides details of the mesh, showing 35 elements across the 0.7 mm slot width, another 100 elements above and below the slot, and 800 elements radially. As little circumferential variation was expected in the flow, only 16 elements were specified in that direction. As with the previous model, the outer surface of the centrebody had a diameter of 25.4 mm, while the inner surface of the annular space had a diameter of 150 mm.

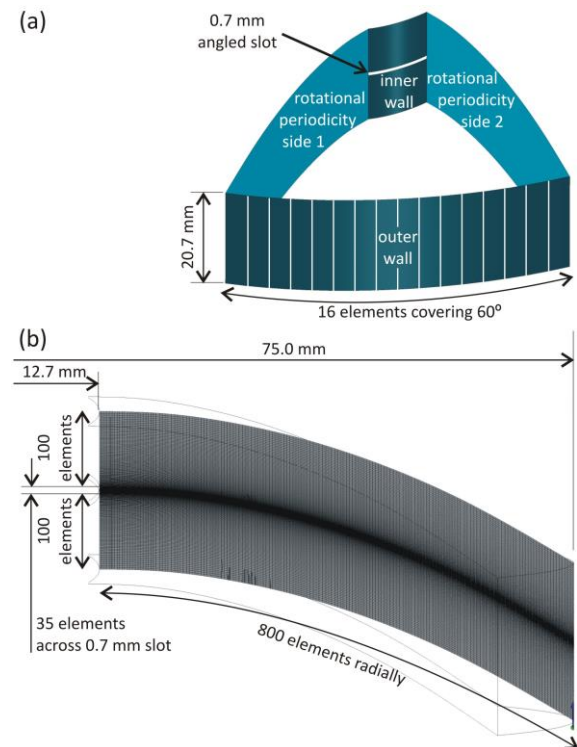


Figure 6: Geometry and mesh dimensions for Liquid Sheet model.

Initially a coarser Cartesian mesh was used to determine the expected location of the film, and then the

fine curvilinear mesh in Figure 6 was created so that the mesh elements could follow the same path as the film.

The film velocity at the slot was specified to be 1 m s^{-1} in the radial direction with zero vertical component of velocity. The boundaries above and below the film were specified as openings at constant atmospheric pressure, while the outer and inner walls had a no-slip wall surface condition. The side boundaries were assigned rotational periodicity boundary conditions so that any fluid flowing out of one boundary would flow back into the flow domain at the other boundary. This feature was important once rotational motion was added to the simulation. In order to simulate rotation of the film, the flow domain could be specified as rotating, and simulations were performed at 0, 100, 200 and 300 RPM.

The liquid flow was assumed to be laminar, since the slot Reynolds number was equal to 786. Standard values of air and water density and viscosity were used in the model. It was found that the results were strongly sensitive to the air-water surface tension specified in the model, and the most reliable way to produce a stable film solution (in agreement with experimental observation) was to neglect surface tension altogether. The issue of surface tension sensitivity is addressed in the Discussion.

A transient solution to the equations of motion were performed with a time step of 0.0005 s , leading to an RMS Courant number of less than 1, indicating time resolution was adequate for the current mesh. A constant time step was used as convergence difficulties sometime occurred when using a variable time step.

Results

The predicted film surface is shown in Figure 7a, as a surface equal to liquid volume fraction of 0.05. The surface is coloured by the local liquid velocity, which starts at 1.0 m s^{-1} at the slot exit and increases slightly towards the outer wall of the device, due to gravitational acceleration. Figure 7b shows an elevation view of the centreline of the film, in this case coloured by liquid volume fraction. The path of the film curves smoothly towards the outer wall of the device, following a parabolic path. The thickness of the film – defined approximately by the number of grid cells that are coloured red and therefore have a liquid volume fraction equal to 1 – reduces with radial distance until about half way to the outer wall of the device. At this point the liquid has diffused across several mesh cells so that no cell is completely filled with liquid. Figure 7c-j shows detail of the film at successive locations along the film, and by position (g) the film is predicted to be smeared over approximately 16 cells, with none of those cells containing only water. At locations h-j a stratification of the film is predicted, with layers of liquid 2-3 cells thick. In Figure 7j the film is shown to hit the outer wall and the volume fraction increases once more to a value of 1.

The numerical diffusion at the top and bottom surfaces of the film is believed to be an artefact of the technique used to define the air-water interface in ANSYS CFX. The stratification shown in Figure 7h-j is also expected to be a result of the numerical techniques, and not a real phenomenon.

Figure 8 shows the film surface at increasing rates of rotation. In order to better visualise the surface of the film, the geometry is repeated six times around the central axis of the device, so that it appears there are six short angled slots around the central tube, each generating its own

liquid film. The film is coloured by the vertical position of the surface to help visualise its shape. The image shows how the leading edge trails the rotating centrebody by increasing amounts with each increase in rotation. However, the actual velocity of individual liquid elements remains radial in direction, as indicated by the vector plot at 300 RPM shown in plan view in Figure 8e. There is a similar issue in prediction of the liquid film surface using a rotating centrebody, in that the film initially is predicted to become thinner with radial distance (like Figure 7c-j) but ultimately spreads out over several mesh elements with water volume fraction less than one.

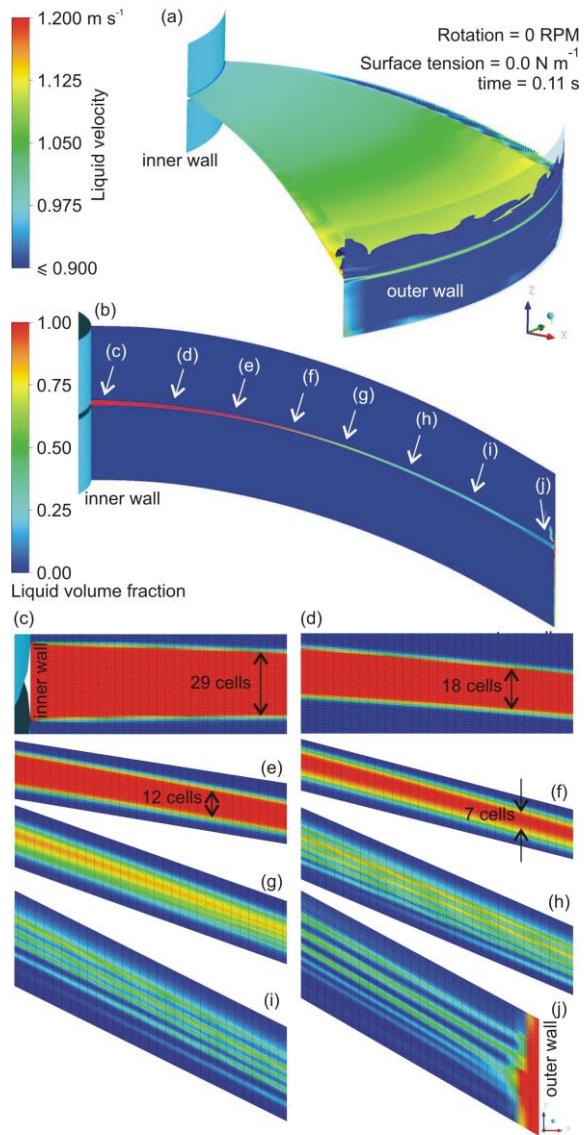


Figure 7: Detail of predicted film surface at 0 RPM. (a) Isometric view; (b) elevation view; (c-j) successive detail of elevation view, showing mesh structure.

A more realistic boundary condition might be to add the circumferential component of rotation at the slot to the liquid velocity. This would presumably predict a straighter leading edge to the film.

The film becomes discontinuous near the outer wall at 300 RPM (Figure 8d) because the rotationally periodic boundaries do not overlap perfectly, but instead one side is higher than the other (see Figure 9a). For the case of 300 RPM rotation, the film exits one periodic boundary

quite high up and then cannot re-enter the opposite boundary as there is no region of overlap between the two at that location (see location of film on the periodic boundary, shown as a thick white line in Figure 9b for 100 RPM rotation, and Figure 9c for 300 RPM rotation).

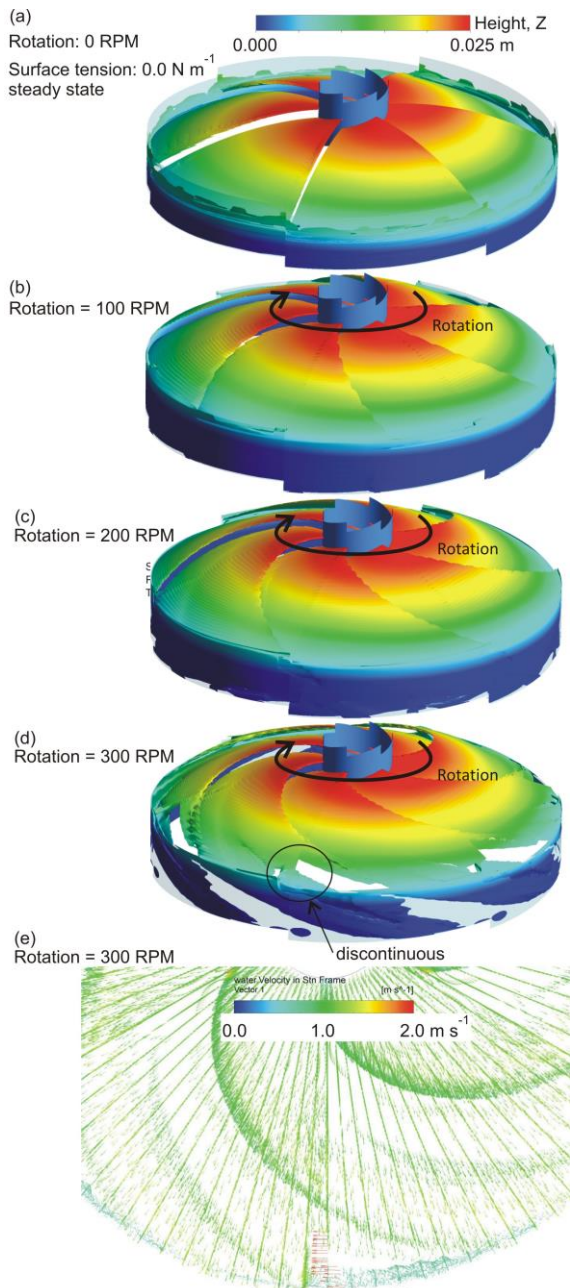


Figure 8: Film surface at (a) 0 RPM; (b) 100 RPM; (c) 200 RPM, and (d) 300 RPM. (e) Plan view of water velocity vectors at 300 RPM.

DISCUSSION – SURFACE TENSION ON THIN FILMS

On addition of surface tension values to the Liquid Sheet model, the model predicts the film to become unstable. Figure 10 shows instantaneous values of the liquid sheet using increasingly large values of surface tension up to the value of 0.072 N m⁻¹ typically quoted for air-water systems. At values of 0.001 N m⁻¹ the film is

generally stable, but has occasional regions of break-up (Figure 10b). Using larger values shows significant breakup of the sheet, in contradiction to experimental observation.

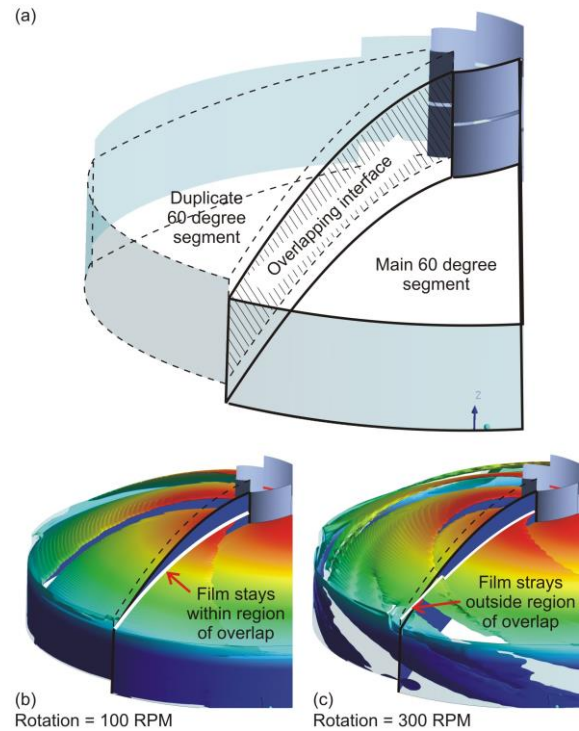


Figure 9: (a) wireframe view of successive 60° segments, showing that periodic boundary interfaces do not overlap perfectly; (b) White line shows film at 100 RPM stays within the overlapping region; (c) White lines show film at 300 RPM strays outside the overlapping region of the periodic boundaries.

Further investigations have been performed to try and understand the cause of this prediction. The system was simplified to one of a downward facing film falling vertically under gravity, and by increasing the resolution of the mesh in all three dimensions it was possible to produce a uniform film with surface tension equal to 0.072 N m⁻¹. However, as soon as the gravity vector is mis-aligned with the direction of fluid entry, the film is predicted to become unstable.

Upon reading the source literature of the ANSYS CFX surface tension model (Brackbill *et al.* 1992) it was thought local radius of curvature effects might be causing difficulties, and it was for this reason that the mesh in Figure 6b was aligned with the direction of film flow. However, even with aligned mesh structure and using a 10° sector (c.f. 60°) with increased resolution it was not possible to predict a stable film. Direct numerical simulation of a round jet by Shinjo (Shinjo and Umemura 2010) has demonstrated that analyses of thin liquid structures such as ligaments and droplets using Brackbill's surface tension model is possible, however they required up to 6 billion elements for their analysis, and claimed that at least 8 cells across any structure was required to produce realistic results. Use of ANSYS FLUENT with volume-of-fluid techniques to determine free surface location, and mesh adaption to maintain resolution of the mesh where required, is being investigated by the authors.

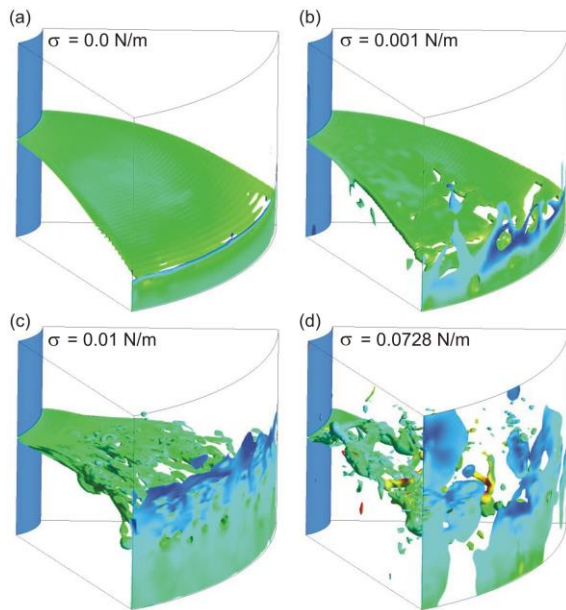


Figure 10: Early simulations of liquid sheet model with increasing values of surface tension.

CONCLUSIONS AND FUTURE WORK

The use of CFD to analyse and understand the operation of a novel gas-liquid contactor has been undertaken. Three separate models of the system were developed in order to break down a complex system into more manageable problems, and the results have generally been in keeping with experimental observation. Ongoing difficulties in predicting surface tension effects on thin films are still to be resolved. Initial work has begun on investigating the mass transfer between gas and liquid in the system, and using ANSYS FLUENT to improve simulation of the film.

REFERENCES

- ANSYS (2013). ANSYS-CFX15.0 User Manual. Canonsburg, PA, USA, ANSYS Inc.
- BRACKBILL, J. U., KOTHE, D. B. and ZEMACH, C. (1992). "A Continuum Method for Modeling Surface-Tension." *Journal of Computational Physics* **100**(2): 335-354.
- DOMBROWSKI, N. and JOHNS, W. R. (1963). "The Aerodynamic Instability and Disintegration of Viscous Liquid Sheets." *Chemical Engineering Science* **18**(3): 203-&.
- SHINJO, J. and UMEMURA, A. (2010). "Simulation of liquid jet primary breakup: Dynamics of ligament and droplet formation." *International Journal of Multiphase Flow* **36**(7): 513-532.
- WARDHAUGH, L. T., ALLPORT, A., SOLNORDAL, C. B. and FERON, P. H. M. (2015). "A novel type of gas-liquid contactor for post-combustion capture cost reduction." *Greenhouse Gases-Science and Technology* **5**(2): 198-209.
- WARDHAUGH, L. T., CHASE, D. R., GARLAND, E. A. and SOLNORDAL, C. B. Gas and liquid phase contactor used in oil and gas industries, has gas inlet that directs gas through gas liquid contacting space into contact with each side of liquid sheets projected from outlets in housing., WO2012103596-A1 (2012).